2017 International Conference on
Unmanned Aircraft Systems (ICUAS)
June 13-16, 2017, Miami, FL, USA

UAV Flight Test Characterization Using Minimal Test Equipment

Brent Michalowski Nathaniel Varano

Aeroprobe Corporation
Christiansburg VA, USA

Abstract— **The aerodynamic performance characteristics of a small UAV were determined using minimal test equipment. Using air data and accelerometer measurement devices it is possible to characterize a UAV airframe using flight test data without the need for any laboratory or wind tunnel support.**

I. INTRODUCTION

A. Background and Motivation

With smaller development budgets, faster design cycles and large variability in size compared to their manned counterparts, the task of characterizing small unmanned aircraft has always been a challenge. Though some experiments can only be performed in a wind tunnel, such as tail off tests, it is not always practical or affordable to test in a wind tunnel. Often, wind tunnels large enough to fit the entire aircraft can be rare and expensive to operate. In many cases the cost of the operational airframe can be comparable to the expense of manufacturing an accurate wind tunnel test model.

With the legalization of commercial UAV use under FAA part 107 in August 2016, the costs and barriers to the entry of flight testing have dropped significantly. While almost every of aspect of the airframe performance can theoretically be analyzed from flight testing, the reality is far more challenging. Flight testing has its own limitations inherited from the flight envelope of the airframe, as well as the limited sensor loadout that can be fitted onboard a small unmanned aircraft. Work has been done on aircraft characterization through flight tests for many years, but with the use of small onboard sensors running at a high rate, it is possible to gather all of the data necessary to characterize any aircraft down to relatively small UAVs without protracted flight maneuvers.

Most autopilot systems on the market are capable of logging accelerometer data, and as the direction of lift and drag are defined by the direction of the airflow, an air data sensor capable of measuring velocity and flow angle is necessary. With these two small sensor suites it is possible to calculate the basic flight characteristics of an airframe.

B. Nomenclature

A: test aircraft wing area
X: body centered axis, positive forward beyond nose
Y: body centered axis, forward though right wing
Z: body centered axis, forward though landing gear
m: mass of test aircraft
C_d : Coefficient of Drag
C_L : Coefficient of Lift
D_a : Accelerometer vector distance from CG
D_p : Probe vector distance from CG
$\ddot{X}\ \ddot{Y}\ \ddot{Z}$: linear accelerometer measurements
α: angle of attack
β: angle of sideslip, X-Z axis projection
β_2: angle of sideslip, X-Y axis
V: airspeed
θ: angle between airflow direction and aircraft X-axis.
ϕ: angle of flow in aircraft Z-X plane
u, v, w : airflow components in body coordinates
u_r, v_r, w_r : measured airflow generated by aircraft rotation

C. Previous Work

Landman explained the benefits of testing the actual aircraft as opposed to a computer or wind tunnel model, which cannot be completely accurate. Some measured quantities, such as control effectiveness, can be extremely sensitive to small changes in the surface and Reynolds number [1].

Faced with the similar issue of limited capacity of onboard sensors for UAV testing, Castillo attempted to use purely internal sensors to attempt to estimate the angle of attack and sideslip. This reliance on accelerometer based systems meant that the actual angle of attack had to be estimated using known aircraft performance. However, when the calculated angle of attack was compared to the measured data, the errors were found to be unacceptably large. This was most likely due to wind variability that could not be accounted for directly [3]. It was determined that a lightweight method of sensing angle of attack and angle of sideslip would be important in aircraft characterization.

Virginia Tech used a combination of CFD, wind tunnel testing and an extensive series of flight tests to characterize the performance and dynamic response of the SPAARO UAV to optimize the autopilot control algorithms. [3]

II. TEST SETUP

For this study, a Finwing Penguin, an off the shelf RC aircraft designed for FPV (first person video piloting), was used. It was chosen due to its extremely stable design, good endurance, low flight speeds, pusher design and large cargo capacity in weight and internal volume. The full technical statistics for the airframe are shown in table 1.

MGTOW	2.8 kg
Empty Weight	1.28 kg
Static Thrust	1.9 kg
Wing Area	0.36 m^2
Wingspan	1720 mm

Table 1: Test Aircraft Specifications

and maximum gross takeoff weight of 2.8 kg, this small aircraft provided an inexpensive off-the-shelf solution for carrying small airborne experiments.

Aeroprobe's Micro Air Data Computer with integrated GPS/INS was able to provide the requisite air data, along with a secondary set of INS information at 20 Hz. The entirety of the sensor suite, including the GPS antenna and multiport probe, weighed in at just over 250g.The full specs of recorded data is shown in table 2. The µADC offered a large savings in weight and a smaller effect on the aircraft flight dynamics, with only a small diameter probe external to the aircraft required, shown in Fig 1.

Recorded Quantities	date, airspeed (V), AoA(α), AoS (β), pressure altitude, air temperature, GPS position, & INS orientation
Max Data Rate	100 Hz
Angle of Attack Range	20°
Angle of Sideslip Range	20°
GPS module	XSens MTi-100

Table 2: Aeroprobe µADC Specifications

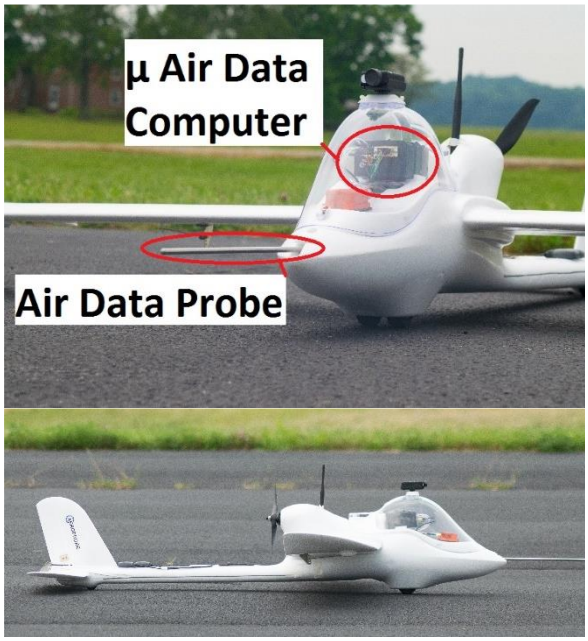

Fig. 1: Front and side view of the test aircraft

Accurately measuring the static pressure of the freestream flow proved to be the most demanding of the testing hardware, requiring a static ring on the nose mounted probe two fuselage diameters, eleven inches, in front of the aircraft. Although this extended the total length of the aircraft by a quarter, there were no noticeable negative effects on aircraft performance.

III. TESTING

The testing was performed under the oversight of the Mid Atlantic Aviation Partnership at Virginia Tech's UAV test facility. An aerial picture of the facility overlaid with the GPS track of one of the flights under manual control is shown in Fig 2.

Through the course of testing, 43,000 data points were taken, excluding those invalidated by anomalous effects, such as ground effect and ground contact.

There are three clear peaks in the flight data shown in Fig 3. The two sharp peaks on the left can be attributed to the time the aircraft spent in an autopilot governed circling loiter, while the less concentrated peak can be attributed to the pilot's manual maneuvering. It is also clear that the average angle of sideslip is approximately –7 degrees. This could be due to P-factor turning the airframe, sensor mounting bias or the pilot and autopilot's favoring of right hand turns.

Flight testing is inherently limited to the aircraft's operational envelope, providing relatively sparse data at extreme flight angles even with aggressive piloting.

Fig. 2: GPS flight path one test flight

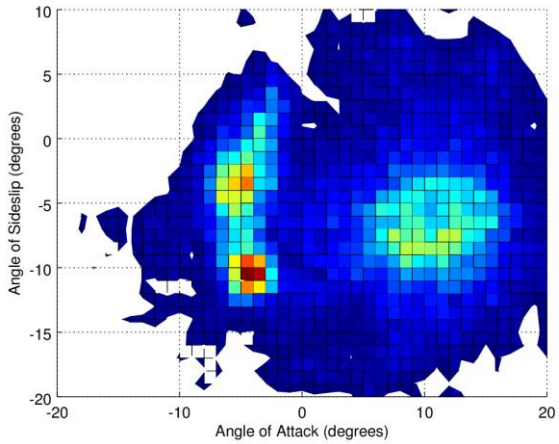

IV. DATA ANALYSIS

To accurately analyze the data taken onboard the aircraft, it is vital to first move all the measurements to the aircraft's center of gravity. In the following equations, a subscript of m (ex: $\ddot{X}_m$) indicates a raw measured quantity while values without can be assumed to be location independent or located at the CG.

As the autopilot in this test was located above and in front of the center of gravity, the recorded linear acceleration contained tangential and centrifugal elements. However, angular rates and accelerations are both recorded by the autopilot and are constant for all locations in a rigid body. Using the distance from the autopilot mounting location and the aircraft's CG ($\vec{D}_a$), as well as the recorded angular rates ($\dot{\theta}$) and accelerations ($\ddot{\theta}$), it is possible to calculate the linear acceleration of the center of gravity using shown in (1).

$$\begin{aligned}
\ddot{X} &= \ddot{X}_m + \vec{D}_a\hat{x} * (\dot{\theta}_y^2 + \dot{\theta}_z^2) + \vec{D}_a\hat{z} * \ddot{\theta}_y + \vec{D}_a\hat{y} * \ddot{\theta}_z \\
\ddot{Y} &= \ddot{Y}_m + \vec{D}_a\hat{y} * (\dot{\theta}_x^2 + \dot{\theta}_z^2) + \vec{D}_a\hat{z} * \ddot{\theta}_x + \vec{D}_a\hat{x} * \ddot{\theta}_z \\
\ddot{Z} &= \ddot{Z}_m + \vec{D}_a\hat{z} * (\dot{\theta}_x^2 + \dot{\theta}_y^2) + \vec{D}_a\hat{y} * \ddot{\theta}_x + \vec{D}_a\hat{x} * \ddot{\theta}_y
\end{aligned} \quad (1)$$

Due to the air data being measured on a boom far in front of the aircraft, the angle of attack and angle of sideslip also had to be corrected by removing the vertical and horizontal measured airflow generated by the aircraft's rate of rotation.

This study uses the angle naming convention of the equipment used, as is shown in Fig. 4. Using this definition, the angle of sideslip is a function of flow velocity in the $\hat{\mathbf{Z}}$ direction, in addition to being a function of flow velocity in the $\hat{\mathbf{Y}}$ and $\hat{\mathbf{X}}$ directions.

To remove the effects of aircraft rotation on air data measurement, the measured flow velocity and angles must first be converted into flow velocity components by using (2).

$$\begin{aligned}
u_m &= V_m * \cos(\alpha_m) * \cos(\beta_m) \\
v_m &= V_m * \sin(\beta_m) \\
w_m &= V_m * \sin(\alpha_m) * \cos(\beta_m)
\end{aligned} \quad (2)$$

Then, using (3), the spurious flow velocity components can be calculated from the distance from the aircraft's center of gravity to the tip of the probe $\vec{D}_p$, and the aircraft rotational rates $\dot{\theta}$.

$$\begin{aligned}
u_r &= -\dot{\theta}_y * D_p\hat{z} + \dot{\theta}_z * D_p\hat{y} \\
v_r &= -\dot{\theta}_x * D_p\hat{z} + \dot{\theta}_z * D_p\hat{x} \\
w_r &= -\dot{\theta}_y * D_p\hat{x} + \dot{\theta}_x * D_p\hat{y}
\end{aligned} \quad (3)$$

The measured airflow generated by aircraft rotation can then be subtracted out from the measured velocities and the airspeed, angle of attack, and angle of sideslip can be recalculated as shown in (4). With the effects of sensor placement removed, it is then possible to use the measurements to characterize the aircraft.

$$\begin{aligned}
V &= \sqrt{(u-u_r)^2 + (v-v_r)^2 + (w-w_r)^2} \\
\alpha &= tan^{-1}(\frac{w-w_r}{u-u_r}) \\
\beta &= sin^{-1}(\frac{v-v_r}{V}) \\
\beta_2 &= tan^{-1}(\frac{v-v_r}{u-u_r}) \\
\phi &= tan^{-1}(\frac{w-w_r}{v-v_r}) \\
\theta &= cos^{-1}(\frac{u-u_r}{V})
\end{aligned} \quad (4)$$

Neither lift nor drag are in a consistent direction in an earth centric or aircraft body centric model, but rather defined as the forces normal to and parallel to the direction of airflow, respectively. However, by using the accelerations recorded onboard the aircraft, and the aircraft's mass to derive the force vector applied to the airframe. The component of this force vector parallel to the measured air data flow vector is drag, whilst the perpendicular component is lift. As the calculation uses only the accelerometer and air data measurements, the effects of gravity, wind and inertia are innately accounted for in the computations.

As the aircraft thrust and its effects are unknown factors and dependent upon throttle setting, battery voltage, airspeed, engine placement and engine alignment, this analysis will be limited to gliding flight to eliminate its effects. Once the characteristics of the aircraft are analyzed in gliding flight, it is possible to use the data to compute the effects of the engine under different conditions, though this is outside the scope of this study. While the lift force is defined as all forces normal to the direction of airflow and all factors are shown in (5), a simplified approach can be taken, as shown in (6).

$$(C_L * \frac{q*a}{m})^2 = (\ddot{X} * sin(\theta) + \ddot{Y} * cos(\beta_2) + \ddot{Z} * sin(\alpha))^2 + (\ddot{X} * sin(\theta) + \ddot{Y} * sin(\beta_2) + \ddot{Z} * cos(\alpha))^2 \quad (5)$$

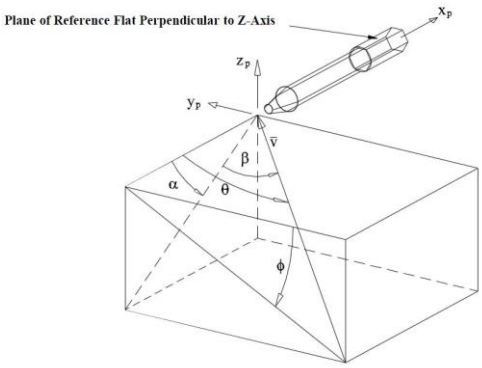

Fig. 4: air data measurement angles

$$C_L = \frac{\ddot{Z} * cos(\alpha) - \ddot{X} * sin(\alpha)}{q * A/m} \quad (6)$$

This set of equations omits both the accelerometer measurements in the Y-direction, as well as removes the effects of angle of sideslip. The omission of these components has very little effect on the calculated lift due to the much lower side area of the aircraft relative to the wing area effective in the Z-direction, and the much lower airspeeds relative to the X-axis. This simplification both reduces the complexity of the data processing, as well as allows the data to be cleanly understood in only two dimensions.

Calculation of the drag force on the aircraft is simply the projection of the vector force on the aircraft onto the direction of airflow, which can be calculated using (7). Lift is slightly more complicated as by its definition, it includes all forces perpendicular to the direction of airflow in (7). The two-dimensional simplification is less applicable for drag calculation as the sideslip component comprises a much larger portion of the drag than it does of the lift.

$$C_D = \frac{\ddot{X} * cos(\phi) + \ddot{Y} * sin(\beta_2) + \ddot{Z} * sin(\alpha)}{q * A/m} \quad (7)$$

V. Results

An initial analysis of the coefficient of lift from the flight test data resulted in an unexpectedly large variance. This was initially accounted for by subdividing the data by elevator setting. Taking only the data from the trimmed elevator setting, the result is shown below in Fig. 5 plotted with the variance. Due to the significantly lower number of data points at extreme angles of attack, the variances are larger at the extremes. Also, the large variance at ten degrees is a clear indication of stall.

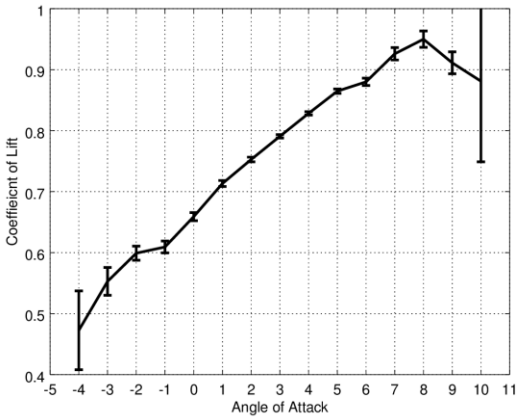

Fig. 5: Zero Elevator Coefficient of Lift and 2σ variance

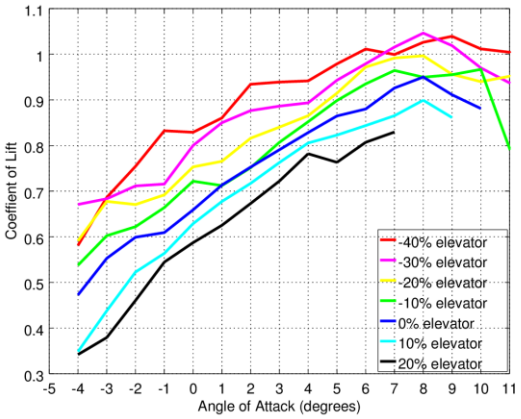

Fig. 6: Coefficient of Lift Divided by Elevator Deflection

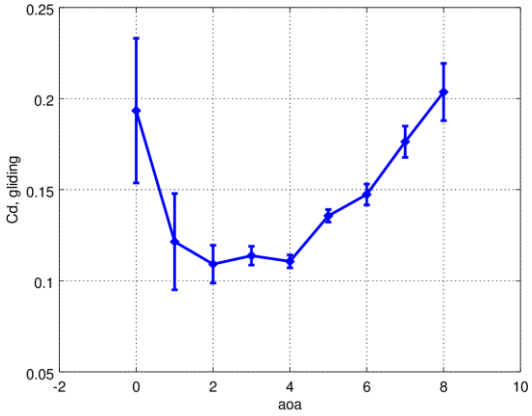

Fig. 7: Coefficient of Drag as a function of AoA with Standard Error

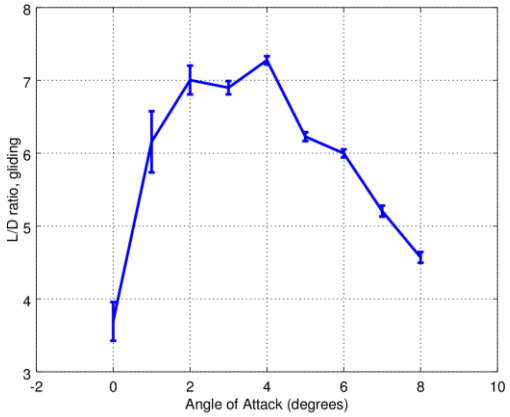

Fig. 8: Lift to Drag Ratio with Standard Error

A comparison of all the elevator settings in Fig. 6 below shows a very strong correspondence between lift and elevator setting. This occurrence is to be expected and well known in its stable condition under the title of trim drag.

The drag was then calculated, shown in Fig. 7. This also proved to match well established trends of aircraft behavior. Unfortunately, the drag measurements contained larger variances than the lift calculations, even after accounting for elevator settings. It would not be out of the question for the engine to still have an effect on this data due to the spin down time of the propeller after the throttle had been reduced to zero, or the effects of a free spinning propeller. While the deviation of the data is significant, the large number of recorded data points allows for a reasonable standard deviation with the data sorted into one degree bins.

Using the calculated lift and drag coefficients, it was then possible to calculate the ratio between them. Fig. 8 shows the lift to drag ratio as a function of angle of attack, showing the best range cruise to be at 2-4 degrees angle of attack.

VI. Conclusion

By the use of an onboard air data system measuring airspeed, angle of attack and angle of sideslip; alongside the measurements recorded by a standard GPS enabled autopilot, it is possible to outline the basic performance characteristics of an airframe.

While wind tunnel testing remains the only way to test individual components, and an advantageous way to test extreme flow conditions, recent advancements have given flight testing the edge in testing full UAV systems. The changes to legislation allow any engineer to become a licensed UAV pilot with relative ease, and conduct the desired testing on their own schedule, independent of any other facility testing schedule or dimensional limits.

VII. Steps toward improvement

It was not acknowledged during the flight testing how critical the gliding data would be for the derivation of aircraft drag, as only 7% of the data taken was while gliding, and only 3% of the data was gliding at a minimal elevator deflection. This limited data set made calculations of drag less reliable. The data could also be filtered to not include data immediately after the throttle was reduced, as well as altering the aircraft to prevent the free spinning of the propeller. A greater emphasis should be given to gliding flight in further flight testing to generate a reliable baseline from which to measure both thrust and control induced drag.

While the physics behind this methodology are sound, verifying the data with proven data will be important. While the airframe inspected in the report has no published data and is too large for most wind tunnels, the same tests can be repeated easily on an airframe with known characteristics.

References

1] Landman D., Britcher C., and Bennett W., “A Power-On Full Scale Win Tunnel Test of a UAV” No. AIAA-A99-33400, AIAA, Chicago, Illinois, 1999.

[2] M. C. Cotting, A. Wolek, J. F. Murtha and C. A. Woolsey, “Developmental flight testing of the SPAARO UAV” in 48th AIAA Aerospace Sciences Meeting Including the New Horizons Forum and Aerospace Exposition, Orlando FL, 2010, doi: AOAA-2010-295.

[3] O. D. Garibaldi Castillo and E. H. Londner “UAV flight testing with an airborne sonic anemometer, IMU and GPS” in 28th AIAA Applied Aerodynamics Conference, Chicago IL, 2010, doi: AIAA 2010-4572.

[4] William Gracey; Measurement of static pressure on aircraft; naca-report-1364; 1958.

[5] Green, Maurice W; Determination of the lift and drag characteristics of an airplane in flight; naca-tn-223; August 1925.